Environmental Sciences Europe

RESEARCH

Open Access

Spatial patterns and bridge collapse interactions of erosional processes due to the 2021 Ahr valley flood

Fabian Weidt[1*], Rainer Bell[1*], Lothar Schrott[1], Alexander Brenning[2], Michael Dietze[3], Lisa Burghardt[4] and Joshua Groeßer[5]

Abstract

The extreme flood event of July 14/15, 2021 caused massive geomorphological changes along the Ahr river in western Germany. The processes include mass movement and bank erosion, channel displacement and widening as well as deposition of material at the floodplains, all of which contributed to extreme damage. However, a comprehensive understanding of the actual control factors and drivers of these processes is lacking. Here, we analyse spatial patterns of erosional processes in three dimensional space and on a regional scale. We quantify bulk volumetric loss in 100 m long and 120 m wide segments along the Ahr river, using a differential terrain model build from pre-event and post-event airborne laser scanning data. We use a multiple linear regression model of net volumetric loss per segment as a proxy of flood power to explore relationships with peak discharge, valley floor width and river curvature. Both volumetric loss itself and the residuals of the regression model are used to examine effects of bridge failure and subsequent outburst waves. The analysis shows that the greatest volumetric loss values are explained by high peak discharges and narrow valley floors. River segments containing destroyed arch bridges show higher volumetric loss than segments with destroyed slab bridges, intact bridges or no bridge at all. These findings suggest that traditional arch bridges may be less effective in preventing the local augmentation of flood power by outburst waves resulting from bridge clogging and failure.

*Correspondence:
Fabian Weidt
f.weidt@geofact.de
Rainer Bell
rbell@uni-bonn.de
[1] Department of Geography, University of Bonn, Bonn, Germany
[2] Department of Geography, Friedrich Schiller University Jena, Jena, Germany
[3] Department of Physical Geography, University of Göttingen, Göttingen, Germany
[4] RWTH Aachen University, Institute of Hydraulic Engineering and Water Resources Management, Aachen, Germany
[5] Paris-Lodron-University of Salzburg (PLUS), Salzburg, Austria

Introduction

On July 13 and 14, 2021, enormous rainfall amounts of 100 to 150 mm fell over western Germany and in parts of Belgium and Luxembourg. Most of the precipitation fell within 15 to 18 h [20], which led to extreme peak runoff conditions along the Ahr river and its tributaries, exceeding mean discharge by factor 150 [28, 29]. Severe geomorphological changes such as mass movement and bank erosion, channel displacement and widening, and the deposition of material on the floodplains were among the consequences [14, 23, 31] (Fig. 1).

Anthropogenic cleaning measures took place rapidly after the event leading to a limitation of the perspective on geomorphological changes as a whole. However, investigating spatial patterns of erosion, quantified as volumetric loss, along the river can help to unravel the

Fig. 1 Channel widening and bedrock erosion at Armuthsbach tributary 300 m upstream of its outlet, located 30 km downstream of the Ahr source. Photography shows post-flood conditions 3 months after the July 2021 event (16 Oct 2021). Post-flood channel width ≈14 m, pre-flood channel width ≈4–5 m. Vertical difference between water level and floodplain ≈1.7 m

spatial variability of flood power, particularly related to river infrastructures. Spatial and statistical analysis can also be used to draw conclusions about general driving mechanisms of extreme flood dynamics.

The causes of severe erosion and deposition during an extreme flooding event involve multiple factors and have been the focus of studies throughout the last decades [2, 3, 15]. However, the destructive nature of flood events, their inaccessibility to classic in-stream survey systems and their often erratic emergence with limited preparation time make it extremely challenging to infer flow parameters such as discharge, velocity, shear stress, or stream power as the events happen. The resulting impact on the shape of the landscape [25] is, therefore, usually assessed from post flood mapping efforts and the construction of scaling relationships between flood magnitude and, for example, the amount of mobilised material. Although such studies on frequency–magnitude relationships have shown a strong connection between moderate floods and sediment transport [35], there is less agreement on the relationship between more extreme floods and geomorphic characteristics. This lack of consensus is partly due to the fact that large floods can sometimes have devastating impacts [2], while other times they only cause minor changes to the landscape [12, 21].

The effectiveness of geomorphic events in molding the landscape is strongly tied to channel boundary shear stress and stream power, which are controlled by flood magnitude, channel morphology, and stream gradient [4]. Peak unit stream power is defined by

$$\omega = \rho_w g Q S w^{-1}$$

where $\rho_w g$ is the specific weight of water in N/m^3, Q is the discharge in m^3/s, S is the slope in m/m, and w corresponds to the water surface width at the cross section.

Based on discharge reconstructions and flood extent mapping [24, 28], surface water width at the cross section is highly determined by valley floor width due to full inundation of riverine floodplains at peak runoff conditions. Following the definition of unit stream power, river sections with high peak discharge and small valley floor widths are expected to show high volumetric loss. This correlation has already been observed and described in a case study by [23]. Conveniently, [31] quantified higher areal percentage of deposition due to reduced flow velocities in areas characterized by low elevation and greater valley width.

Lateral erosion was also apparent in several reaches of the meandering Ahr river, predominantly on the outer side of a bend, the cut bank [7]. With increased discharge, shear stress increases so that more material is eroded from the cut bank and transported downstream. River sections with high channel curvature, serving as proxy for strong relative shear stress are presumed to show high volumetric loss values.

Bridges represent a direct restriction of the runoff cross section due to bridge piers, abutments and superstructure. Accordingly, bridge structures have been shown to exert a strong control on flood discharge patterns during the 2021 flood event [30]. Floating debris that got trapped caused further narrowing of discharge cross sections at bridges by clogging. This constriction caused the water levels upstream of the bridge structures to rise, in some cases leading to significant ponding effects [8]. According to initial estimates, the water level of the flood wave was increased by up to three meters due to the clogging at bridge structures [30]. The sudden failure of individual bridges led to additional flood waves that carried higher volumes of water and floating debris [8]. Due to the resulting outburst flood waves, volumetric material loss is expected to be higher in areas downstream of destroyed bridges, even though significant erosion processes were also observed upstream of some bridges [7, 23].

[36] reviewed that a surprising amount of bridges were destroyed by hydraulic mechanisms, mainly including flood and scour but the vulnerability of bridges to floods has received little attention compared to other hazards such as earthquakes [32]. Flooding can lead to the collapse a bridge in various ways, such as scour, sand missing, softened bedrock, erosion, insufficient embedment depth, river convergence, debris impact or abrasion on bridge foundations, etc. [36]. As a result,

robust and validated methodologies for the flood fragility and vulnerability assessment of bridges are scarce, although some attempts to develop such methodologies were recently made, with the aid of expert judgement or numerical modelling. Hydraulic loads on bridges due to flotsam accumulation and backwater rise were not considered or their importance underestimated in previous design approaches [9, 32].

[22] put forward a formal elicitation process to identify bridge vulnerability factors, summarizing the current knowledge of the problem of scour from various experts in the field. Not surprisingly, the foundation depth, type, and level of uncertainty in the estimation of these quantities emerged as the most important factors that should be considered when assessing bridge flood vulnerability and risk. However, the bridge type was ranked only 16th as a vulnerability factor, which is quite interesting given the very different behaviour and capacity to withstand scour of a masonry arch bridge compared to a bridge with a multi-span simply supported deck.

[9] analyzed the correlation between bridge design and the overtopping and clogging of bridges during the 2021 flood event. Overtopping of bridges (whether induced by clogging or not) resulted in major bridge damages but also damages to the surrounding area. Differences within statistical analysis of three investigated rivers (Ahr, Inde and Vicht) indicate that, in general, many factors determine the damage pattern and the destruction of a bridge structure. Data suggests that the extent of damage decreased with an increasing number of bridge piers. For the shape of the opening no statistical correlation could be observed along the three rivers, since bridges with a rectangular opening were more dominant along the rivers Inde and Vicht and, therefore, no representative distribution was derived. Similar to [22] and [32] they concluded, that the bridge type was not a decisive factor in the damage to a bridge during a flood.

This work attempts to draw conclusions about additional hydraulic forces by quantifying volumetric changes in proximity to bridges. Due to the resulting outburst flood waves, volumetric loss is expected to be higher in areas downstream of destroyed bridges, even though significant erosion processes were also observed upstream of some bridges [7, 23]. Corresponding to the well-known positive correlation between unit stream power and sediment transport, it is expected that this effect can be observed more frequently at high peak discharge and narrow valley width. In this regard, [34] have also recently shown that the evolution of mud deposits and stagnant water pools was in relation to driftwood and infrastructure systems, such as bridges and concrete bank structures, particularly in areas with narrower valley floors.

Using a multiple linear regression model, peak discharge, valley floor width and river curvature are controlled as explanatory variables for volumetric loss allowing an adjusted assessment of river segments adjacent to bridges. The aim of this study is to identify spatial patterns of volumetric loss and derive a relation between this variable and bridge construction types, damage grades, and discharge conditions during the mid-July 2021 flooding event in the Ahr Valley. We consider volumetric loss as a proxy for flood power. This is evaluated based on the following three research questions:

(1) Are peak discharge, valley floor width and/or river curvature significant linear explanatory variables for riverine volumetric loss in the Ahr valley in the 2021 event?
(2) Is volumetric loss augmented in river segments in proximity to bridges?
(3) Does this correlation depend on damage grades or bridge construction types?

Methods and data

Study area

The Ahr river has a length of 85 km and is located in the Eifel low mountains in western Germany. The catchment has an area of close to 900 km^2 and contributes left-sided to the Rhine river discharge. The valley slopes are predominantly forested, while the valley floor is mostly grassland and, after entering the Rhine valley, arable land [16]. [23] classify the Ahr and its catchment into four subsections due to their heterogeneous geomorphological characteristics. The upper reaches show a hilly landscape with little relief and a smoothly meandering river course. The bed material is characterized by siliceous fluvial gravel [34]. The middle course of the Ahr begins in Müsch, 20 km downstream of the source. Here the river has cut 200–300 m deep into the bedrock and shows characteristic incised meanders. From Kreuzberg near Altenahr (km 50), there is an increase in the slope gradient and a marked reduction in the valley floor width. Shale is present in the river bed [34]. From Walporzheim (km 68), the valley widens in a funnel shape to a wide alluvial plain that merges into the lower terrace of the Rhine at Sinzig. Within the channel, fine material accounts for a larger proportion of fluvial sediments [34].

From 12 to 15 July 2021, the Ahr river catchment received partially rainfall up to 150 *mm* (Fig. 2). The orographic conditions, the lack of retention areas, sealed urban areas and dense population, in conjunction with the high moisture content of the soil and the enormous amounts of precipitation, were the main factors causing the flooding [5].

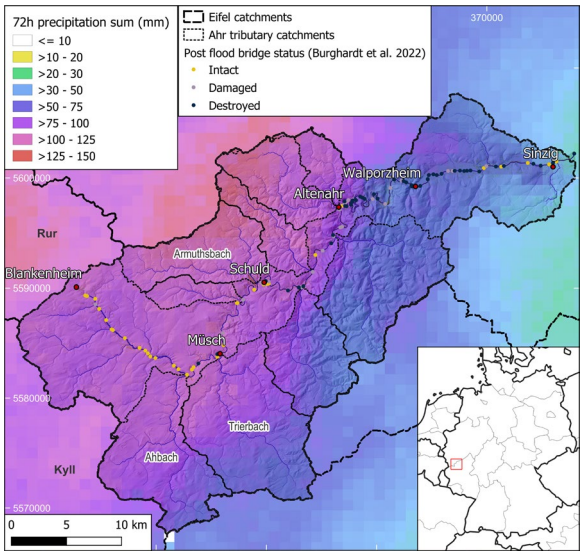

Fig. 2 Ahr valley catchments and 72 h precipitation sum from 2021-07-12 05:50 to 2021-07-15 5:50 UTC derived from RADOLAN data product SF [33]. Terrain data source: [19]. Bridge mapping: [8]

The interaction of the fast moving flood water with landscape elements and the debris, sediment, and wood it carried were also responsible for the flood's devastating impact, which, therefore, was challenging to predict [14]. Coarse material and woody debris were introduced into the channels, causing a series of consequences. The channel thalweg was displaced laterally or even the entire main stem was relocated within the floodplain in many cases, altering the local gradient. Furthermore, the trunk stream was blocked, at least temporarily, in some instances [14]. Large woody debris played a critical role in altering the flood non-linear [13] and hamper the prediction, from small headwater channels down to the main streams. The transport of large woody debris through the river channels had various consequences. When the debris got stuck in obstacles, such as bridges, the water flow was obstructed, leading to temporary ponding and backwater effects in the main streams. Consequently, the water levels upstream increased, causing the inundated areas to expand until the obstacle was either bypassed, overtopped, or destroyed. In the latter case, a pulse of water could travel downstream, resembling an outburst flood [14].

The Ahr river's eight main tributaries are the Ahbach, Trierbach, and Armuthsbach in the upper catchment, and the Adenauer Bach, Liersbach, Kes-selinger Bach, Sahrbach, and Vischelbach in the central catchment. Only smaller tributaries contribute to the lower catchment area. Particularly for the Armuthsbach, a major impact on the discharge in the Ahr main channel is indicated by a peak discharge reconstruction by [28], intense areal precipitation [33] and the occurrence of massive changes in channel morphology near its outlet in Schuld (Fig. 1, 2).

In this study, the subdivision of the Ahr valley used by [23] is supplemented by a boundary in the village Schuld as an attempt to consider different magnitudes of peak discharge.

A detailed assessment of bridges in the Ahr main valley including damage grades and construction types has been carried out by [8]. At the 2021 event, there were a total of 114 bridges along the Ahr. Bridges with round or oval passages were classified as arch bridges, bridges with almost rectangular openings were mostly represented as slab bridges. Bridges with further classifications referring to bridge superstructures as well as bridges with unspecified type or damage grade are not considered in this study. Three bridges in Blankenheim (Ahr source village) and the autobahn bridge in Sinzig mark the borders of the area of interest (AOI) and are excluded due to no expected effect on runoff and erosion processes. The twin viaduct in Altenahr and two adjacent unspecified bridges are also disregarded, since a road tunnel breakthrough of a meander bend has caused complex runoff conditions leading to vertical erosion at the downstream tunnel exit in a range of $2\,m$ to $8\,m$ [23]. This leads to an analysis of 74 bridges, grouped into 39 arch bridges and 35 slab bridges based on labels by [8]. In the upper and lower reaches, there were mostly slab bridges, while in the middle reaches the number of arch bridges was predominant (Fig. 3). From km 30 onwards, the majority of bridges got damaged or destroyed during the July 2021 event. The amount of bridges labelled as completely destroyed is equal in terms of construction type.

Data acquisition Geomorphological changes are quantified using a differential terrain model based on pre-event and post-event digital terrain models (DTMs). For pre-event morphology, data was acquired in routine airborne laserscanning campaigns of the surveying services of the federal states of Rhineland–Palatinate and Northrhine–Westfalia.

These DTMs are provided with a ground sampling distance of 1 m [17, 18] with horizontal accuracies of ± 0.3 m and vertical accuracies of ± 0.15 m. They display conditions of the year 2019 (km 20–km 50), 2018 (downstream of km 50) and 2016 (km 0–km 20). Post-event data was gathered from mid-September to end of October 2021 by an airborne laserscanning campaign, commissioned by [6]. To create a differential raster, this post-event DTM with a GSD of $0.5\,m$ and a horizontal and vertical accuracy of ± 0.15 m is resampled by local averaging to 1 m GSD to match the pre-event data set.

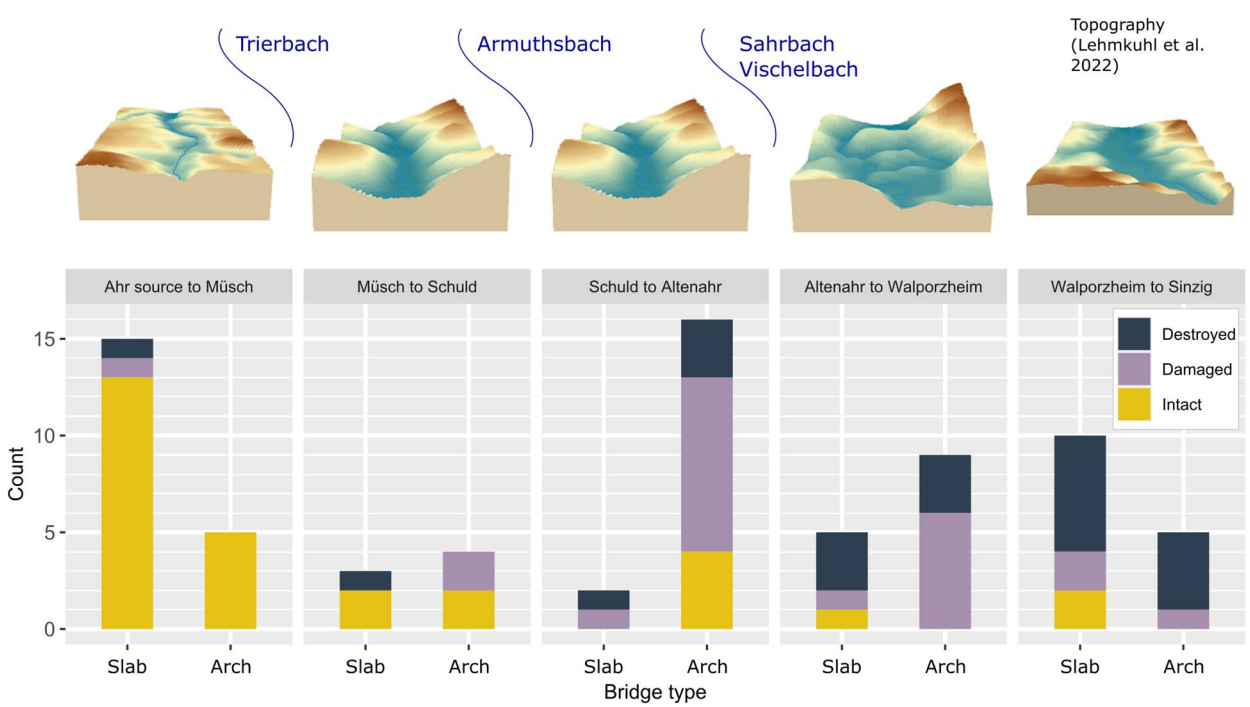

Fig. 3 Distribution of bridge types in Ahr river sections. Sections based on morphological characteristics [23] and conceivably different magnitudes of unit stream power variables peak discharge and valley floor width. Sectionwise distribution of investigated bridge types and damage grades is plotted using a data set first discussed in [8]. Bridges showing no damage or only decorative or weathering-like damage have been assigned as 'Intact'. Bridges that were completely destroyed and wrenched off by the flood event are classified as 'Destroyed'. Thus, the class 'Damaged' covers a broad range of flood imprints from limited usability due to loss of railings to extreme risk of stability after subsidence or displacement of the piers. Topographic block models by [23]

Positive values in the differential raster are assumed to indicate a net gain of material, negative values represent net erosion. However, changes in the channel are may be biased by water level differences, since the laser pulse is primarily reflected at the water surface. To some extent, the time lag between the two data sets and the event limits the confidence in attributing the observed change solely to the event. However, since no other larger flood occurred in this period and due to the extreme magnitude of the flood event most of the major changes in the selected buffer zones of the river (see below) are most likely caused by the 2021 event. Clean-up measures implemented promptly resulted in large artificial accumulations of various types of transported material. Thus, with regard to the direct flood impact we assume net erosion in the data sets to be more reliable than net gain of material. To account for these limitations, we limit our analyses to areas with negative DTM differences, which we refer to as *volumetric loss*.

Data editing To perform multivariate statistical analysis, differential raster data is vectorized by using a two sided buffer around the river centerline, subdivided every 100 m. This divides the river longitudinally into 844 equally sized segments with a length of 100 m and a fixed segment width. For each segment, the sum of negative terrain differences represents the total amount of volumetric loss. With increasing segment width, the increase in volumetric loss diminishes at distances > 60 m to the river, and artefacts of human activity may have an increasing influence on volume estimates. We, therefore, choose a fixed segment width of 120 m in this study, i.e., 60 m distance each side (Fig. 4).

The grid allows an investigation of morphological changes in the longitudinal course of the river using the distance from source as the unique spatial coordinate of any segment. Information about status and construction type of contained bridges per segment is obtained from [8] point data. This enables, for example, the calculation of the mean volumetric loss of all segments located 200 m downstream of a segment containing a destroyed slab bridge.

Explanatory Variables Peak discharge, valley floor width and river curvature are considered as predictor variables in modeling volumetric loss. Using the residuals of a multiple linear regression model for subsequent analysis, the impact of these predictors is aimed to be

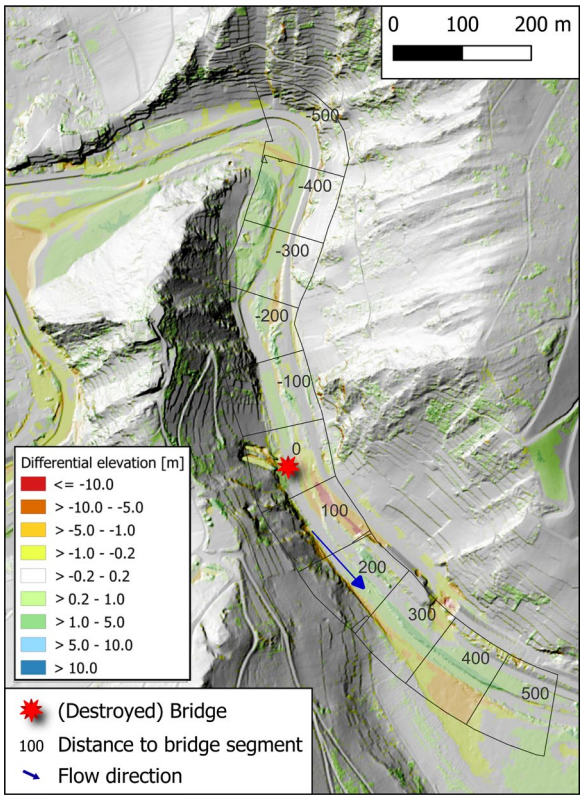

Fig. 4 Sampling grid with 100 m long and 120 m wide segments. Within each grid segment, the volumetric loss is defined as the zonal sum of negative elevation differences. Hillshade and differential terrain model based on [17, 18] (pre-event) and [6] (post-event)

eliminated to focus on possible effects of bridges. Ideally, the residuals of a good model with high explanatory power for volumetric loss could point out data anomalies resulting from effects (e.g., bridge failure) that are not reflected by the model's predictors.

For the 2021 event, peak discharge at the Ahr main channel had been reconstructed at seven survey sites by [28] using an indirect estimation method. Runoff Q is computed on the basis of an empirical uniform-flow equation (1) involving channel characteristics, water-surface profiles, and a roughness coefficient

$$Q = \frac{1}{n} A R^{\frac{2}{3}} S^{\frac{1}{2}}. \quad (1)$$

Here, R is the hydraulic radius in m, which is the ratio of the cross-sectional area A and the wetted perimeter U. S is the energy-line slope in m/m, and n the dimensionless hydraulic roughness coefficient according to Manning.

The approach is applied to an actual cross-sectional geometry obtained from a local geodetic survey. The position of peak flow marks limits the drained area. Field work took place in the summer of 2021. Four major work steps were performed at all sites: The identification and survey of peak flow marks, the survey of the cross profile, the determination of roughness coefficients (based on [1, 10]), and the assessment of channel slope. To guarantee an error-minimal reconstruction of the peak discharges, [28] made several demands on the study sites. House walls in the entire catchment area showed signs of flooding, but the actual maximum water level may have been overestimated due to factors, such as capillary rise and wave run-up. Obstacles like bridge piers caused impoundments, further exaggerating water levels. To mitigate these potential inaccuracies, study sites were selected outside of settlements and with ample distance from bridges. Since peak discharge reconstructions are only available for a limited number of study sites, point data from [28] is inter- and extrapolated along the distance from source using simple linear regression. The model is based on seven survey profiles achieves a high accuracy ($R^2 = 0.97$).

Continuous valley floor width data is obtained from the 2021 post-flood DTM [6] using the algorithm of [11]. To identify floodplain and terrace regions, the method calculates two metrics for each pixel in the raster: First, the elevation of the pixel in relation to the closest channel and second, the local slope. For a pixel to be categorized as floodplain or terrace, both the elevation and slope metrics must fall below a predefined threshold. Setting this threshold values manually is recommended by [11] for lower-relief landscapes. Taking suggested values from [11] and visual interpretation of different results into account, a slope threshold of $0.1\,m/m$ and a relief threshold of $35\,m$ is selected for deriving widths of the Ahr main channel valley floor in a few meters sampling distance. To address an overestimation of valley width due to meandering rivers, [11] suggest using a valley centerline extraction method instead of relying solely on the steepest-descent trace. This approach is adopted for the Ahr river due to various meandering sections. By visual interpretation of the hillshade DTM and the flood water impact line [24], further areas with overestimated valley floor widths were identified and manually corrected. This applies in particular to the areas at tributary mouths where, in addition to the main valley, areas of tributary valleys are mistakenly included by the algorithm.

Cut bank structures are modelled using short-range river curvature as a basic proxy variable. It is expected that in sections with higher curvature, cut bank structures are present and thus, higher volumetric loss values occur.

The applied metric for river curvature of a specific segment is the difference in the cardinal directions of flow routes from previous to following segment. Smoother metrics using larger survey distances from tested segments (see dashed arrows in Fig. 5 for a two-segment

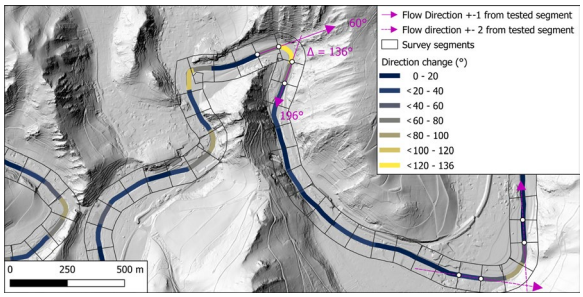

Fig. 5 Example showing the calculation of river curvature. Considering flow direction change from previous and following segment as explanatory variable for volumetric loss (top center) leads to a similar goodness-of-fit of the regression model ($R^2 = 0.016$) as a larger distance between the segments (as shown in the bottom right)

distance) were rejected after reviewing model accuracy of simple regression models of volumetric loss.

Results

Observational Data A positive trend in volumetric loss magnitude as a function of segment distance from source is clearly visible in an exploratory analysis (Fig. 6). Peak values are reached between Altenahr (50 km) and Walporzheim (70 km), partially associated with destroyed or damaged bridges. *z*-scores of volumetric loss exceed one from 30 km onwards and between Altenahr and Walporzheim several times even three, indicating highly anomalous losses. The absolute maximum at 56.5 km reflects the massive vertical erosion at the Altenahr tunnel exit with a volumetric loss of over 20000 m^3 in a single 100 m segment. This segment is excluded from the sampling range for subsequent assessment of bridge-loss interaction.

The valley floor widens from nearly 250 m in the headwaters up to nearly 500 m between Schuld and Altenahr. Widths decrease to less than 20 m in the Langfigtal conservation area between Altenahr and

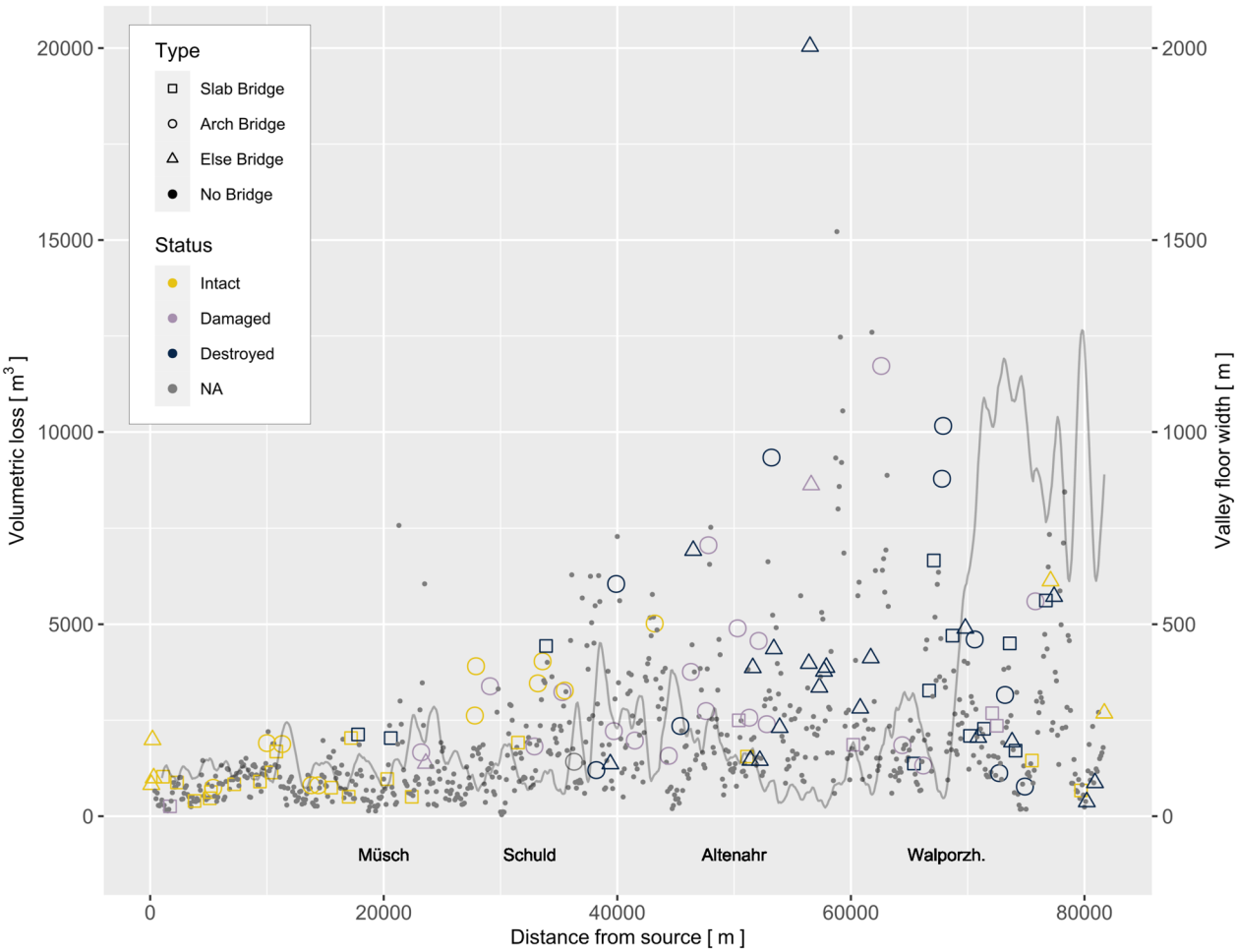

Fig. 6 Volumetric loss per 100-m river segment. Segments containing a bridge are labelled by construction type and damage grade. Continuous valley floor width data shown as grey line (10-segment rolling mean). Locations of survey section borders are indicated

Walporzheim (52 km from source), in incised meanders. The water gap in Walporzheim is indicated by a sharp minimum followed by a rise of the width up to > 1 km. It is noticeable that two destroyed arch bridges show considerably high volumetric loss values. In the lower reaches, in contrast, volumetric losses fall below 5000 m^3 except for a section in Heimersheim around km 77, where topography is characterized by a narrowing of the floodplain.

Predictors

Pearson's correlation coefficient $r = 0.38$ of interpolated peak discharge and volumetric loss is weak to moderate, but significant (nominal p value < 0.001). Valley floor width shows peak values in the lowest ranges, but in the whole data set there is no significant correlation (nominal p value 0.85). River curvature, quantified by direction change, correlates weakly, but significantly (nominal p value < 0.001) with volumetric loss. All p values may be affected by violated assumptions due to serial autocorrelation and heteroscedasticity.

Considering the predictors peak discharge, valley width and river curvature and their pairwise interaction in a multiple linear regression model, 23% of the variance of volumetric loss can be explained (Tab. 1). Only peak discharge has a significant effect on volumetric loss, modified by river curvature and valley width. A lower valley width is associated with a significant (nominal p value 0.044) increase in the positive effect of peak discharge on volumetric loss. River curvature has a significant (nominal p value 0.012) amplifying effect on the influence of peak discharge as an interaction variable (Fig. 8).

Model residuals are used for further analysis to remove the effects of these predictors and focus on additional factors. Heteroscedasticity and non-normal distribution are still present for the residuals (Fig. 7, Tab. 1).

Residuals Model residuals still show heteroscedasticity with a maximum variance in the Altenahr–Walporzheim section (Fig. 9).

Bridge segments in the Schuld to Altenahr section with low loss values (lower quartile) are frequently located in the widest floodplains (upper quartile) and contain damaged arch bridges. In the confined Altenahr–Walporzheim section, three destroyed arch bridges are located in outlier sections in terms of residual loss and below the median valley floor width. In the lower reaches, destroyed bridges are frequently present in the upper half of residual loss values.

When considering all type–status combinations, destroyed arched-bridge segments ($n = 10$) solely show a significant negative correlation between valley floor width and residual loss ($r = -0.6$, p value 0.039), indicating that the effect of a bridge on erosion decreases for wider floodplains. The majority of destroyed bridges of both types is located in the wide valley section downstream of Walporzheim. In the upstream section, there are generally more arch bridges, but they were predominantly not destroyed. Since the distribution of peak discharge and valley width data indicate a reduction of unit stream power in Walporzheim, we suggest that bridge failure may be in causal relation to higher volumetric loss.

Bridge neigbourhood analysis For each combination of the bridge variables 'Type' and 'Status', the segments are grouped by their distance to the respective bridge segment. Mean values of residual loss for each group show that in arch-bridge segments the residual loss rises in comparison with upstream segments. For destroyed bridges of this type, the true mean is with 95% confidence within an interval > 0 (see errorbar in Fig. 10).

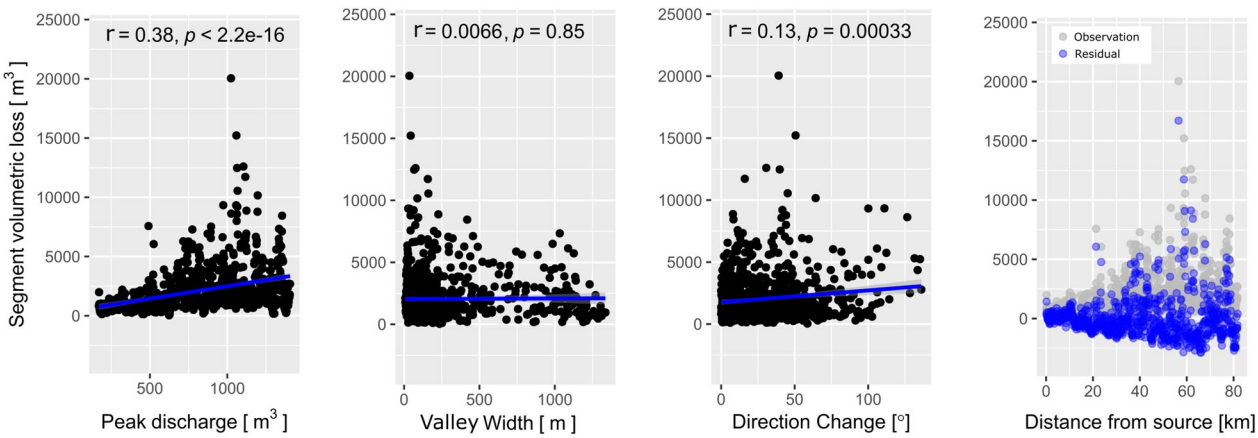

Fig. 7 Predictor variables of the multiple linear regression model for volumetric loss with Pearson's correlation coefficient r. Nominal p values of correlation tests must be handled with care due to violation of assumptions. Right: Regression residuals plotted against distance from source

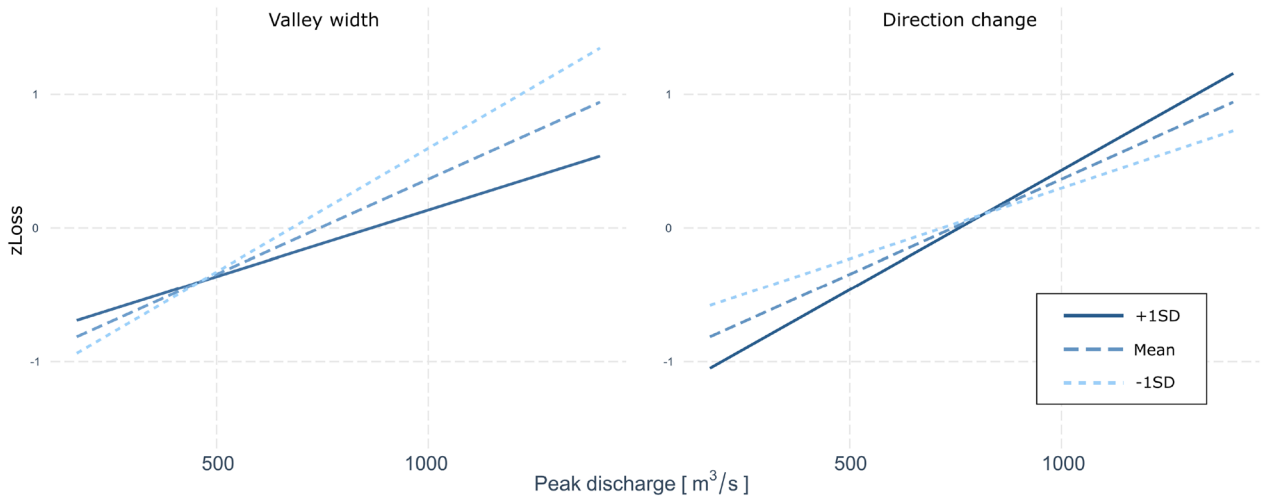

Fig. 8 Interaction effects of valley width and direction change on the predictor peak discharge for *z*-standardized volumetric loss (both *p* values < 0.05). Lower valley floor width the effect of peak discharge on volumetric loss. The opposite applies for direction change, a proxy for cut bank structures

Table 1 Multiple linear regression model summary for volumetric loss using *z*-standardized predictors peak discharge, valley floor width and river curvature ($R^2 = 0.24$, adjusted $R^2 = 0.23, F(7, 809) = 35.72, p < 0.001$). Asterisk (*) indicates interaction term

Variable	Estimate	Std. Error	p value
(Intercept)	0.0634	0.0506	0.2101
Peak discharge	0.5080	0.0493	< 0.001
Valley width	− 0.1404	0.0965	0.1462
Direction change	− 0.0105	0.0569	0.8541
Peak discharge*Valley width	− 0.1526	0.0756	0.0438
Peak discharge*Direction change	0.1302	0.0517	0.0119
Valley width*Direction change	− 0.1367	0.1025	0.1828
Peak discharge*Valley width*Direction change	0.0200	0.0841	0.8125

This peak weakens until from 200 m downstream a more or less stationary level of 500 m^3 volumetric loss is reached. Even in the −100 m group the value is increased compared to upstream segments. For damaged arch bridges the rise from −100 to 0 is not as prominent as for intact arch bridges. For slab bridges, only the destroyed ones show a remarkable, but not significant rise in the bridge-containing segments. All other group means are not significant.

A sectionwise look at all bridges in detail (Fig. 11) reveals that in the Altenahr–Walporzheim section large and isolated amplitudes in bridge segments are observed for three destroyed and one damaged arch bridge (partly torn Nepomukbrücke in Rech). Two of the destroyed bridges are located near Walporzheim. In one of these two segments, the differential DTM indicates cut-bank erosion without high river curvature. The third one is located in a curved segment at the Altenahr tunnel entrance. Between Schuld and Altenahr, almost every arch bridge indicates a spike in residual volumetric loss in the central segment followed by a decrease to +1 and intermittent pattern downstream. However, only one of three destroyed slab bridge shows a remarkable increase, reaching its top in the +1 downstream segment. This segment marks the outlet of the Adenauer Bach (creek) in Dümpelfeld. In the lower reaches, the arch bridges show generally lower residual values and two of five bridges with a peak in residual loss in the central segment.

Slab bridges are frequently present in the headwaters and in the lower reaches. Three destroyed slab bridges in the lower reaches show a (smoothed) spike in the central segment with a magnitude similar to arch bridges in this river section. Here, all four non-destroyed slab bridges show small positive (damaged) or even negative (intact) residuals. In the confined Altenahr–Walporzheim section, three railway bridges are aligned downstream of Marienthal. The third one, a slab bridge at the Kleinod restaurant, was destroyed by the flood and is associated with the only sharp increase of residual loss among all slab bridges in this section.

Spatial prediction of destroyed bridges

The data can also be used to predict if a bridge is destroyed. From this, we can, furthermore, get information on which variables are associated with an increased probability of destruction of a bridge. We

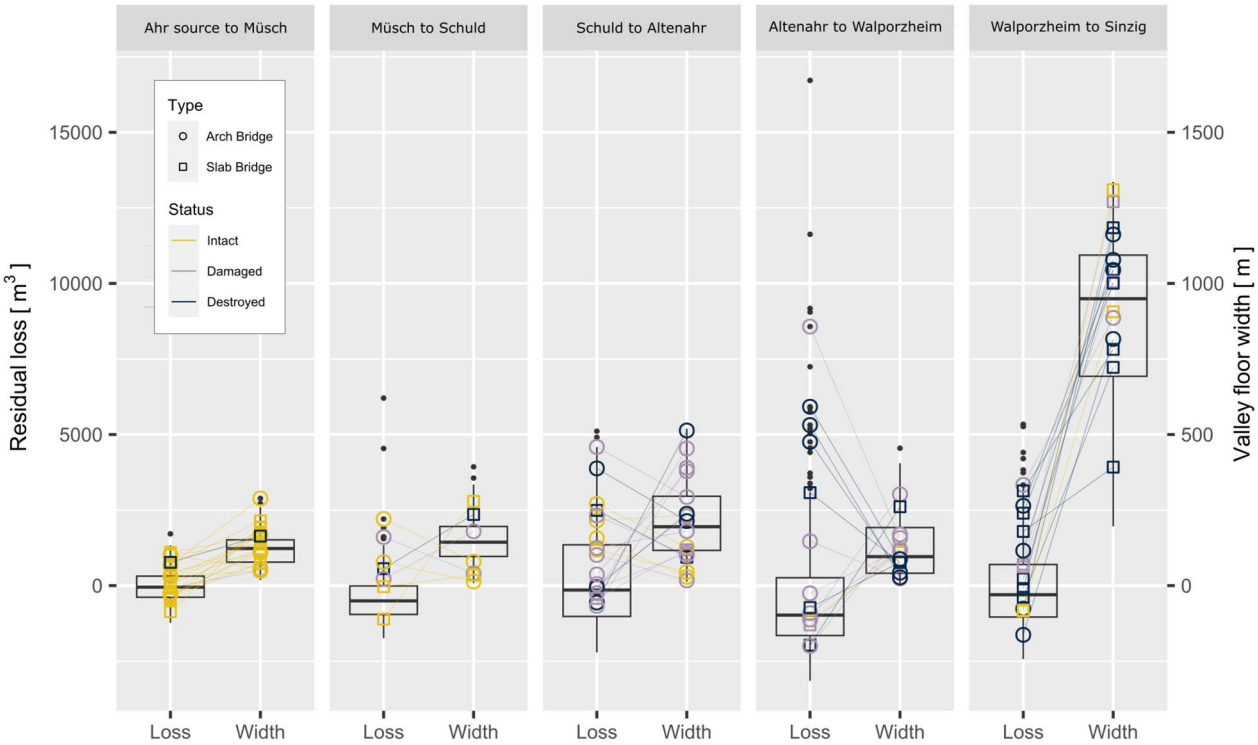

Fig. 9 Ahr river sectionwise residual volumetric loss and valley floor width distribution. Residual loss is based on data correction by multiple linear regression model with predictors peak discharge, valley floor width and flow direction change (Fig. 7). Segments containing a bridge are labelled by construction type and damage grade. Outliers are defined by data exceeding 1.5 times interquartile range

used a logistic regression model for the prediction and tested it with all possible combinations of explanatory variables, choosing the model with minimal Akaike information criterion (AIC). The best results where obtained when choosing distance from the source and valley floor width, leading to a prediction with balanced accuracy of 0.75 and $\kappa = 0.47$. However, when we restrict the data to sections where the valley is especially narrow (valley floor width < 100 m; predictor valley floor removed), we obtain even better results (Fig. 12). This model achieves a balanced accuracy 0.91 and $\kappa > 0.818$.

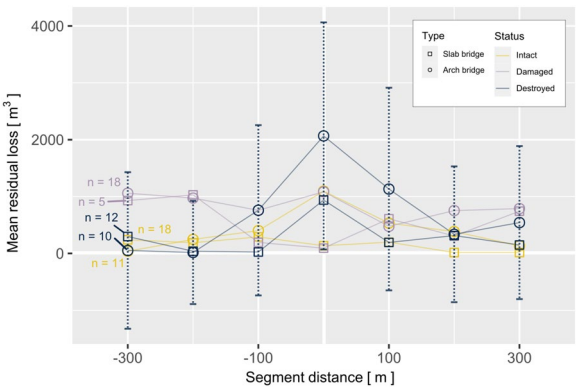

Fig. 10 Segment mean residual loss grouped by distance from bridge. For every bridge, segments within a radius of 500 m upstream and downstream are grouped and analyzed. The error bar indicates a 95% confidence interval of adjacent segment group means of destroyed arch bridges

Discussion

Given data from [28, 29], it is appropriate to use distance from source as a proxy for peak discharge. However, for the multiple linear regression model, linearly interpolated values of peak discharge are used. Since [28, 29] reconstructed peak discharge for only seven profiles sites along 90 km of stream length, the validity of the interpolation must be handled with care.

Post-flood digital terrain data offer a limited view on flood-induced geomorphological processes due to rapid anthropogenic cleaning measures prior to data collection. Nevertheless, the focus on volumetric loss as a proxy for flood power provides a new perspective on the interactions between transverse anthropogenic structures and the river's morphological responses to the flood.

Peak discharge has moderate explanatory power for volumetric loss. It is capable of explaining a positive downstream trend, but extreme amplitudes of

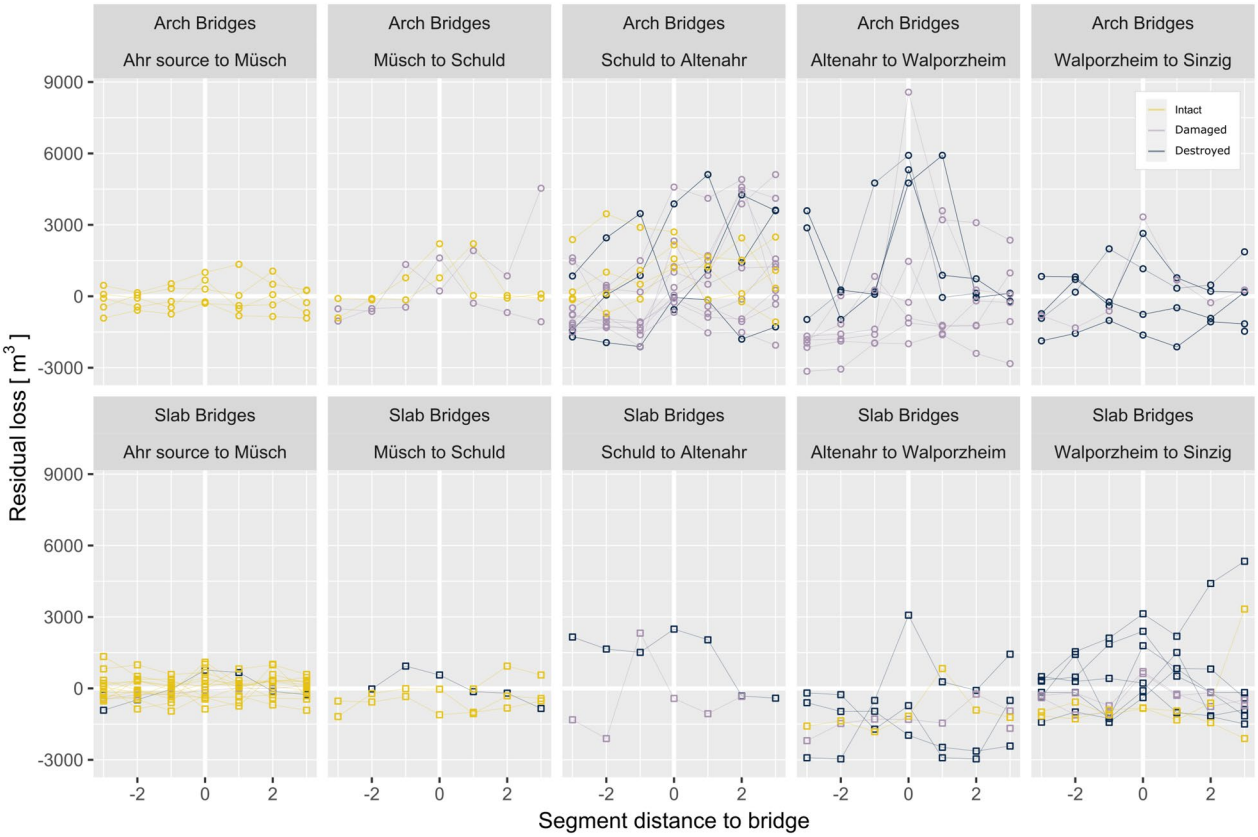

Fig. 11 Bridge-specific residual loss three segments upstream and downstream of bridges. Data is subdivided according to segmentation by [23] supplemented by a data split in Schuld (mouth of the Armuthsbach tributary)

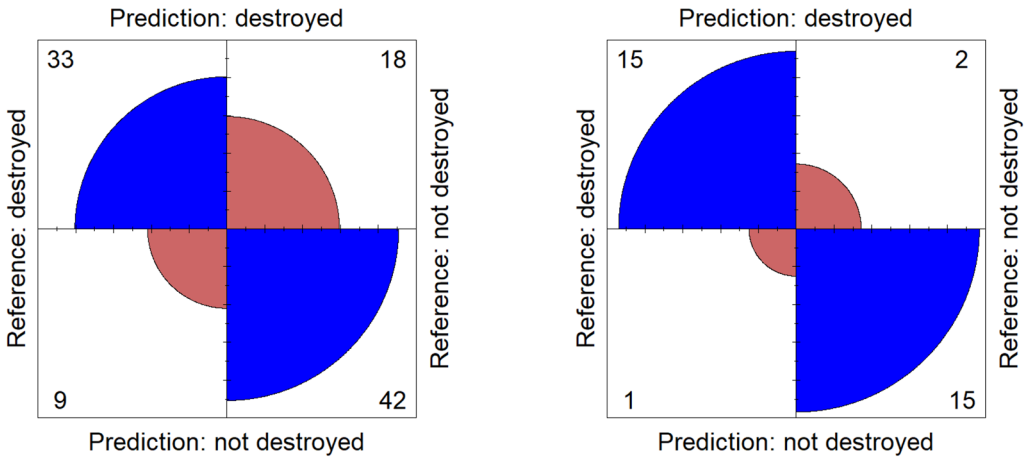

Fig. 12 Left: Spatial prediction of destroyed bridges (using the full data set). Right: Prediction of destroyed bridges in narrower sections with a valley floor width < 100 m

volumetric loss cannot be explained only by considering peak discharge as a linear predictor. Besides other investigated predictors, non-linearities of peak discharge conditions must be taken into account. The doubling of volumetric loss values downstream from Schuld, km 32 (Fig. 6) indicates that the Armuthsbach catchment might have had a remarkable impact on discharge and geomorphological processes in the

main valley. Field observation of large-scale erosion processes at the Armuthsbach (Fig. 1) confirm the pattern visible in volumetric loss data of the main valley. These findings suggest that peak discharge at Armuthsbach could have surpassed the reconstructions of [28, 29], who calculated a peak discharge of 200 m^3/s for the tributary and 625 m^3/s in the Ahr river in a village (Fuchshofen) upstream of the tributary mouth. In contrast, the location of the Sahrbach outlet (km 50), for which [28, 29] reported peak discharges of a similar magnitude as for the Armuthsbach, does not mark an increase in volumetric loss values in the main channel, at least until the narrowing of the Ahr valley from km 53 onwards. This could be explained by a loss of flood power by dense settlement in this area. However, all previous reasoning is also dependent from unclear variables such as the temporal relation of peak discharges of the tributary and in the Ahr main channel. Hydrologic modelling could help to resolve this issue.

Valley floor width has only low explanatory power for volumetric loss. Valley width is low in the headwaters and in the middle reaches. Low explanatory power might result from unexplained variations in peak discharge. Valley floor width acts as an interacting 'moderator' variable for peak discharge as a predictor of volumetric loss (Fig. 8). The same applies for river curvature, quantified as direction change. Higher curvature leads to a stronger effect of peak discharge on volumetric loss. A lack of accuracy of the linear model for curvature as a predictor for volumetric loss might result from simplicity of the curvature model. Morphological properties like elevation differences of cut bank structures or lithology are not taken into account.

It is noticeable that the majority of the segments containing a bridge are located in the upper half of the residue distribution of the respective sections. In line with this, [31] identified increased erosion in the proximity of one bridge at km 67.8 using a differential elevation model.

The finding that segments with damaged and destroyed bridges often display high residual values allows two different conclusions to be drawn. Either the bridges have been damaged by the generally extreme discharge conditions and damage/failure are a kind of side effect, or the failure of the bridge itself caused additional forces, proxied by high volumetric loss. [31] adress the amplified erosive effects at km 67.8 to bridge blocking and failure based on field observations.

In terms of mean values, destroyed bridges are associated with an increased residual loss in the segment of the bridge and a reduction in the following 200 m downstream (Fig. 10). [26] found a similar pattern in data from reconstructed peak discharge after an extreme flood in a small tropical basin in September 2005. They reported that the collapse of an about 4 m high jam during the Rio Portalon flood event may have caused a small surge wave followed by a sudden drop in estimated peak discharges typical of small dam breaches in mountain rivers. However, the flow surge associated with their collapse is very unlikely to have determined the flood itself, whose catastrophic consequences can be traced to the severity of the precipitation event [26].

Here, significance of the increase in segments with destroyed arch bridges must be treated with caution, as only very little data is available. In addition, the mean values are distorted by individual extreme values in the Altenahr–Walporzheim section (Fig. 11). From this perspective, a causal relationship between peak discharge and the destruction of a bridge cannot be identified with certainty. However, the distance from the source as proxy for the peak discharge gives us a remarkably good prediction of bridge destruction on the whole data set and especially in the narrower parts. Even more, in those parts, all other potential explanatory variables from our data set become negligible.

As we have seen, valley morphology rapidly changes in Walporzheim from confined topography to a wide floodplain. When considering all type–status combinations, only destroyed-arch-bridge segments ($n = 10$) show significant correlation between valley floor width and residual loss ($r = -0.6$, p value 0.039). The majority of destroyed bridges of both type is located in the wide valley section downstream of Walporzheim. In the (confined) upstream section, there are generally more arch bridges, but they were predominantly not destroyed. Since the distribution of peak discharge and valley width data indicate a reduction of unit stream power from Walporzheim onwards, this metric does not seem to be a major causal factor leading to bridges to collapse. It seems more plausible to conclude that bridge failure had a causal influence on morphological processes. However, it must be taken into account that the wide valley floor from Walporzheim onwards is a densely built area. Discharge conditions in this section were heavily affected by anthropogenic structures and artificial channel morphology.

Data indicates descriptively that large-scale processes rather occur where an arch bridge collapses, but the sample size is rather small and to make this finding more robust, other variables such as bridge height and the number of bridge piers and passages must be taken into account in further local studies. Recent work of [9] showed in a study of the 2021 event that for the design parameters bridge length, width, clear opening width and number of spans no significant statistical correlation could be found for the degree of damage at a bridge.

They pointed out that bridge height could be determined as a contributing factor influencing the extent of damage more than the shape of the opening of the bridge (e.g., bridge type). However, [9] outline a lack of representatively distributed data and emphasize that statistical analysis has been performed without considering structural design, hydraulic conditions and geotechnical aspects. This study fills parts of this research gap by considering hydraulic conditions proxied by volumetric loss. [27] point out that flood hazard mapping procedures carried out without taking into account stochastic processes at critical cross sections (e.g., bridges) can result in erroneous evaluations, especially in forested basins whose channels naturally transport high wood loads. For further approaches dealing with hydrological modeling data, a nested approach entailing deterministic simulations as well as stochastic evaluation is recommended to achieve a more reliable determination of flood hazard areas and the associated risk. All in all, a recommendation for a flood-adapted bridge construction method cannot be drawn from this work, as the data available is too limited. A multidisciplinary approach taking into account diverse engineering and geoscientific concepts and perspectives is desirable for the resilient construction of river structures in the Ahr valley and other flood-prone regions.

Conclusion

The results of this work clearly indicate an extreme magnitude of hydrological and geomorphological processes of the July 2021 event in the Ahr valley. Doubling volumetric loss values from Schuld (km 32) downstream show a prominent influence of the discharge of the Armuthsbach catchment on the magnitude of processes in the main valley. A closer examination of processes in the Armuthsbach catchment may be advisable to further flood protection measures in this catchment area. Further work could also take a closer look at the relationship between peak discharge and volumetric loss at the other tributaries with high reported peak discharges, at least at the Sahrbach.

In the main valley, peak discharge is a significant linear predictor for volumetric loss, in contrast to valley floor width and river curvature. Nevertheless, these two variables both act as moderators of the peak discharge–loss relationship (Fig. 8). The volumetric loss data set provides evidence that supports the hypothesis of an amplification of geomorphic change due to the failure of obstacles and resulting outburst waves. Data suggests that arch bridges are spatially more strongly associated with higher magnitudes of volumetric loss than slab bridges; however, neither the causality of the relationships nor a general statement about a more flood-favorable bridge construction method can be derived with certainty from our results. A subsequent local-scale analysis which incorporates other bridge properties such as height or observed clogging and other local factors such as geology might be interesting for subsequent work. Thanks to [8], detailed information about the post-flood bridge conditions in the Ahr valley exists. Approaches using concepts of time series analysis could be used to deal with heteroscedacity and autocorrelation of data, but first investigations incorporating AutoRegressive Integrated Moving Average (ARIMA) and Generalized AutoRegressive Conditional Heteroscedasticity (GARCH) components did not lead to better modeling results.

The July 2021 flood was undoubtedly an event that caused severe geomorphological changes in the Ahr valley. As tragic as the 2021 event was, it will hopefully serve a series of research projects to better understand the dynamics of floods in densely populated regions.

Author Contributions

Fabian Weidt, Rainer Bell wrote the main part of the manuscript. Alexander Brenning contributed to statistical analysis. Micha Dietze contributed to gaining and processing of ALS terrain data rapidly after the 2021 event. Lisa Burg-hardt provided information of bridge types and status in the Ahr valley and added engineering knowledge. Josh helped with statistical questions and wrote the prediction of bridge failure subsection. All contributing authors revised the manuscript.

Funding

Open Access funding enabled and organized by Projekt DEAL.

Availability of data and materials

Data and code are made available upon reasonable request. Availability of data is partly subject to authorization by third parties. No data sets were generated or analysed during the current study.

Declarations

Competing interests

The authors declare that they have no Conflict of interest.

Received: 31 May 2024 Accepted: 19 May 2025
Published online: 02 June 2025

References

1. Arcement G, Schneider V. Guide for selecting Manning's roughness coefficients for natural channels and flood plains. Number 2339 in Water Supply Paper. USGS, (1989)
2. Baker VR (1977) Stream-channel response to floods, with examples from central Texas. Geol Soc Am Bull 88:1057–1071
3. Baker VR (1994) Geomorphological understanding of floods. In: Morisawa M (ed) Geomorphology and Natural Hazards. Elsevier, Amsterdam
4. Baker VR, Costa JE (1987) Flood power. In: Mayer L, Nash D (eds) Catastrophic Flooding Binghamton Geomorphology Symposium. Routledge, London
5. Bell R, Kron W, Thiebes B, Thieken A. Die Flutkatastrophe im Juli 2021 in Deutschland. In Die Flutkatastrophe im Juli 2021 in Deutschland - Ein Jahr danach: Aufarbeitung und erste Lehren für die Zukunft. Deutsches Komitee Katastrophenvorsorge e.V. (DKKV), 07. ISBN 978-3-933181-72-5. DKKV Schriftenreihe 62 (2022)

6. Brell M, Roessner S, Dietze M, Bell R, Magnussen S, Schreck D, Jany S, Ozturk U, Merz B, Thieken A. Eifel Flood (2021) - Airborne Laser Scanning (ALS) and Orthophoto Data. GFZ Data Services. 2023
7. Brüll C, Esser V, Lehmkuhl F, Schulte P, Wolf S. Geomorphologen und Wasserbauingenieure betrachten die Auswirkungen des Juli-Hochwassers. RWTH-Themen : Forschungsmagazin, 2021: 12–17, 2021. ISSN 0179-079X. https://doi.org/10.18154/RWTH-2022-01162. URL https://publications.rwth-aachen.de/record/840269. Accessed 28 Feb 2025
8. Burghardt L, Schüttrumpf H, Wolf S, Klopries E (2022) Analyse der Schäden an Brückenbauwerken in Folge des Hochwassers 2021 an der Ahr. Wasser und Abfall 24:12–17
9. Burghardt L, Klopries E-M, Schüttrumpf H (2025) Structural damage, clogging, collapsing: Analysis of the bridge damage at the rivers Ahr, Inde and Vicht caused by the flood of 2021. J Flood Risk Manag 18(1):e13001. https://doi.org/10.1111/jfr3.13001
10. Chow VT (1959) Open-Channel Hydraulics. McGraw-Hill, New York
11. Clubb FJ, Weir EF, Mudd SM (2022) Continuous measurements of valley floor width in mountainous landscapes. Earth Surf Dyn 10(3):437–456. https://doi.org/10.5194/esurf-10-437-2022
12. Costa JE, O'Connor JE (1995) Geomorphically Effective Floods. Geophys Monogr Series 89:45–56. https://doi.org/10.1029/GM089p0045
13. Dietze M, Ozturk U (2021) A flood of disaster response challenges. Science 373(6561):1317–1318. https://doi.org/10.1126/science.abm0617
14. Dietze M, Bell R, Ozturk U, Cook KL, Andermann C, Beer AR, Damm B, Lucia A, Fauer FS, Nissen KM, Sieg T, Thieken AH (2022) More than heavy rain turning into fast-flowing water - a landscape perspective on the 2021 Eifel floods. Nat Hazard Earth Syst Sci 22(6):1845–1856. https://doi.org/10.5194/nhess-22-1845-2022
15. East A, Logan J, Mastin M, Ritchie A, Bountry J, Magirl C, Sankey J (2018) Geomorphic Evolution of a Gravel-Bed River Under Sediment-Starved Versus Sediment-Rich Conditions: River Response to the World's Largest Dam Removal. J Geophys Res: Earth Surf 123:3338–3369
16. Bundesamt für Naturschutz. Landschaftssteckbrief Ahrtal. https://www.bfn.de/landschaftssteckbriefe/ahrtal, 2023. Accessed 10 Mar 2023
17. GeoBasis-DE / LVermGeoRP. Pre-flood digital terrain model of Rhineland-Palatinate (1m). https://lvermgeo.rlp.de/de/produkte/geotopografie/3d-geodaten/digitale-gelaendemodelle-dgm/, 2023. Accessed 28 Feb 2025
18. GeoBasis-NRW. Pre-flood digital terrain model of Northrine-Westfalia (1m). https://www.bezreg-koeln.nrw.de/geobasis-nrw/produkte-und-dienste/hoehenmodelle/3d-messdaten, 2023. Accessed 28 Feb 2025
19. Japan Aerospace Exploration Agency. ALOS World 3D 30 meter DEM. V3.2, Jan 2021. Distributed by OpenTopography. https://doi.org/10.5069/G94M92HB, 2021. Accessed 27 Apr 2023
20. T. Junghänel, P. Bissolli, J. Dassler, R. Fleckenstein, F. Imbery, W. Janssen, F. Kaspar, K. Lengfeld, T. Leppelt, M. Rauthe, A. Rauthe Schöch, M. Rocek, E. Walawender, and E. Weigl. Hydro-klimatologische Einordnung der Stark- und Dauerniederschläge in Teilen Deutschlands im Zusammenhang mit dem Tiefdruckgebiet "Bernd" vom 12. bis 19. Juli 2021. https://www.dwd.de/DE/leistungen/besondereereignisse/niederschlag/20210721_bericht_starkniederschlaege_tief_bernd.html, 2021. Accessed 3 May 2023
21. Kochel RC (1988) Geomorphic Impact of Large Floods: Review and New Perspectives on Magnitude and Frequency. In: Baker V, Kochel R, Patton P (eds) Flood Geomorphol. Wiley, New York, pp 169–187
22. Lamb R, Aspinall W, Odbert H, Wagener T (2017) Vulnerability of bridges to scour: insights from an international expert elicitation workshop. Nat Hazard Earth Syst Sci 17(8):1393–1409. https://doi.org/10.5194/nhess-17-1393-2017
23. Lehmkuhl F, Kessels J, Schulte P, Stauch G, Dörwald L, Wolf S, Brüll C, Schüttrumpf H (2022) Beispiele für morphodynamische Prozesse und Verlagerungen in Folge des Hochflutereignisses 2021 im Ahrtal. Wasser und Abfall 24:40–47. https://doi.org/10.1007/s35152-022-1349-7
24. LfU. Hochwasser im Juli 2021. Technical report, Landesamt für Umwelt Rheinland-Pfalz, Mainz, 2022. https://lfu.rlp.de/fileadmin/lfu/Wasserwirtschaft/Ahr-Katastrophe/Hochwasser_im_Juli2021.pdf. Accessed 15 Apr 2023
25. Magilligan FJ, Buraas EM, Renshaw Carl (2015) The efficacy of stream power and flow duration on geomorphic responses to catastrophic flooding. Geomorphology 228:175–188. https://doi.org/10.1016/j.geomorph.2014.08.016
26. Mao L, Comiti F. The effects of large wood elements during an extreme flood in a small tropical basin of Costa Rica. volume 67, pages 225–236, 05 (2010). ISBN 9781845644420. https://doi.org/10.2495/DEB100191
27. Mazzorana B, Comiti F, Volcan C, Scherer C (2011) Determining flood hazard patterns through a combined stochastic-deterministic approach. Nat Hazard 59(1):301–316. https://doi.org/10.1007/s11069-011-9755-2
28. Roggenkamp T, Herget J (2022) Hochwasser der Ahr im Juli 2021 - Abflussabschätzung und Einordnung. Hydrol Wasserwirtsch 66(1):40–49
29. Roggenkamp T, Herget J (2024) Flood reconstruction - The unexpected rather frequent event at River Ahr in, (2021). Glob Planet Change 240:104541. https://doi.org/10.1016/j.gloplacha.2024.104541
30. Schüttrumpf H, Birkmann J, Brüll C, Burghardt L, Johann G, Klopries E-M, Lehmkuhl F, Schüttrumpf A, Wolf S. Herausforderungen an den Wiederaufbau nach dem Katastrophenhochwasser 2021 in der Eifel. volume 68 of Dresdner Wasserbauliche Mitteilungen, pages 5–16. 45. Dresdner Wasserbaukolloquium 2022, Dresden (Germany), 14 Jun 2022 - 15 Jun 2022, Technische Universität Dresden, (2022)
31. Steinritz V, Bellanova P, Schmidt B, Schüttrumpf H, Schwarzbauer J, Reicherter K, Geomorphic changes after the, (2021) Central European flood in the Ahr valley by LiDAR-based differences. Environ Sci Eur 36(1):12024. https://doi.org/10.1186/s12302-024-00893-x
32. Tubaldi E, White CJ, Patelli E, Mitoulis SA, de Almeida G, Brown J, Cranston M, Hardman M, Koursari E, Lamb R, McDonald H, Mathews R, Newell R, Pizarro A, Roca M, Zonta D (2022) Invited perspectives: Challenges and future directions in improving bridge flood resilience. Nat Hazard Earth Syst Sci 22(3):795–812. https://doi.org/10.5194/nhess-22-795-2022
33. Wetterdienst D. RADOLAN hourly/daily precipitation sum. https://www.dwd.de/DE/leistungen/radolan/radolan_info/home_freie_radolan_kartendaten.html, 2023. Accessed 14 Feb 2025
34. Wolf S, Stark N, Holste I, Lehmkuhl F, Römer W, Burghardt L, Schüttrumpf H (2024) Evaluation of the high-energy flood of mid-July 2021 as a morphologic driver in the anthropogenically developed Ahr Valley, Germany, in interaction with infrastructures. Environ Sci Eur 36(1):54. https://doi.org/10.1186/s12302-024-00860-6
35. Wolman G M, Miller John Preston (1960) Magnitude and Frequency of Forces in Geomorphic Processes. J Geol 68:54–74
36. Zhang G, Liu Y, Liu J, Lan S, Yang J (2022) Causes and statistical characteristics of bridge failures: A review. J Traffic Transp Eng 9(3):388–406. https://doi.org/10.1016/j.jtte.2021.12.003. (**ISSN 2095-7564**)

Publisher's Note